Journal of Low Temperature Physics, Vol. 30, Nos. 1/2, 1978

Ultrasonic Dispersion and Attenuation Near the Liquid–Gas Critical Point of ^{3}He*

David B. Roe and Horst Meyer

Department of Physics, Duke University, Durham, North Carolina

(Received June 20, 1977)

We report ultrasonic dispersion and attenuation measurements near the liquid–gas critical point of ^{3}He at frequencies from 0.5 to 5.0 MHz and densities from $0.89\rho_c$ to $1.15\rho_c$. The singular part of the sound attenuation and the dispersion on the critical isochore $\rho_c = 0.0414$ g/cm^3 are analyzed in terms of the Kawasaki–Mistura theory. If the Ornstein–Zernike order parameter correlation function is assumed in the analysis, good agreement with our data is achieved, except close to the critical temperature T_c in the high-frequency region, where $\omega^* = \omega/\omega_D \gg 1$. Here ω_D is the characteristic relaxation rate of the critical fluctuations. From a fit of the theory to our data, and assuming the inverse correlation length κ is expressed by $\kappa = \kappa_0\varepsilon^\nu$, where $\varepsilon = (T-T_c)/T_c$ with $\nu = 0.63$, we obtain $\kappa_0 = (3.9 \pm 0.4) \times 10^9$ m^{-1}. It is found that a more realistic form of the correlation function, as proposed by Fisher and Langer and calculated by Bray, yields even poorer agreement with out data than does the classical Ornstein–Zernike form for $\omega^* > 10$. The same difficulties appear in the analysis of the available data for xenon. Thus, the present mode coupling theory is unable to satisfactorily describe the acoustic experiments on fluids near the liquid–vapor critical point over a large range of reduced frequencies ω^*. In the appendix, we reanalyze previously reported ultrasonic data in ^{4}He, taking into account the nonsingular term of the thermal conductivity. Using $\nu = 0.63$, we obtain a good fit of the experiment to the theory in the hydrodynamic region with $\kappa_0 = (5.5 \pm 1) \times 10^9$ m^{-1}.

1. INTRODUCTION

Sound propagation has proven to be a valuable tool in the investigation of dynamic behavior of systems near critical points. For instance, near the liquid–gas critical point of a monatomic pure fluid, the very large sound attenuation and velocity dispersion are caused by hysteresis energy loss when the decay rate ω_D of density fluctuations becomes on the order of the

*Supported by a grant from the National Science Foundation.

0022-2291/78/0100-0091$05.00/0

sound wave frequency $\omega/2\pi$. There are two frequency and temperature regions with very different behavior of the attenuation and dispersion: the low-frequency hydrodynamic region, where $\omega \ll \omega_D$, relatively far from the critical point, and the high-frequency nonhydrodynamic region, where $\omega \gg \omega_D$, very close to the critical temperature T_c. In this paper we present dispersion and attenuation data for ^{3}He in both these regions and analyze them in terms of the Kawasaki[1] formalism. A comparison with several forms of the order parameter correlation function is made, taking into account several modifications of the classical Ornstein–Zernike (OZ) form. Furthermore, a reanalysis of earlier acoustic experiments in ^{4}He is presented in the appendix.

We have measured the sound velocity and attenuation as a function of temperature at six densities near the critical point of ^{3}He, but in this analysis we will concentrate on the critical isochore $\rho = \rho_c = 0.0414$ g/cm^3. The frequency range investigated was from 0.5 to 5.0 MHz, and the temperature ranged from $T_c = 3.3$ K to 3.7 K, the critical temperature being 3.3083 K.

This is a continuation of our earlier work in ^{4}He,[2] which we were able to compare with low-frequency acoustic experiments[3] and light scattering experiments.[4–6] Xenon has also been thoroughly investigated by low-frequency acoustics,[7] ultrasonic,[8–11] Rayleigh scattering,[12] and Brillouin scattering [13,14] experiments. Experiments in monatomic fluids have generally been interpreted in terms of the Kawasaki[1] mode coupling calculation of attenuation and dispersion due to the divergence of the bulk viscosity. The rederivation by Mistura[15] in terms of a frequency-dependent specific heat and the modification of these results to correct for large dispersions[9] have been extensively used.[2,11,16] Unfortunately, when the OZ form for the order parameter correlation function is used in these calculations, the results contradict experiments[2,9,11] in the extreme nonhydrodynamic region.

Kawasaki[17] has shown that if a better form for the correlation function is assumed, the calculated attenuation and dispersion have approximately the same temperature and frequency dependence as found by experiments in the extreme nonhydrodynamic region. Kawasaki calculated only the limiting high-frequency behavior, though, and no explicit expression was given for the attenuation and dispersion over the entire frequency and temperature range. The validity of Kawasaki's arguments has been tested in xenon by Tartaglia and Thoen,[16] who fit the existing data to the theory using the OZ correlation function in the hydrodynamic region. In the high-frequency region they used a modification of the Fisher–Langer[18] form for the correlation function. We shall come back in some detail to the basic problems encountered with this comparison in the high-frequency region.

In this paper, we will show that the Kawasaki–Mistura calculations assuming the OZ correlation function fit well the acoustic data in ^{3}He in the

hydrodynamic region if the hyperscaling value $\nu = 0.63$ (using $\alpha = 0.11$)[19] is assumed. The magnitudes of the correlation length and thermal conductivity found in this fit are on the order of those expected from other experiments. We have also attempted to compare our data with the Kawasaki–Mistura expressions using the Fisher–Langer correlation function in the non-hydrodynamic region. The intermediate region $\omega/\omega_D \gtrsim 10$ has a quite different behavior than is actually observed if the correct sign of the leading order correction term, as calculated by Bray[20] or Fisher and Aharony,[21] is used. In order to achieve a good fit to our data, the opposite sign must be used. This unphysical sign has also been assumed in the analysis[16] of the xenon data, as we shall explain below.

2. EXPERIMENTAL PROCEDURE

The ultrasonic measurements were carried out with the same acoustic etalon and cryostat as was used to measure the dispersion and attenuation in ^{4}He, and which is described in Ref. 2. The sample chamber, to be described below, contained two X-cut quartz transducers separated by a few millimeters of fluid ^{3}He through which the sound pulses traveled. The velocity and attenuation measurements were made by observing the time of flight and the amplitude of the pulse after it has passed through the fluid. The ultrasonic cell was strongly thermally coupled to a ^{4}He reservoir near the ^{3}He critical temperature. Its temperature, which was controlled electronically to within 20 μK, was measured by a germanium resistance thermometer calibrated against the ^{4}He vapor pressure scale. Since the sample chamber, acoustic techniques, and cryostat have been previously described, only the changes pertinent to this experiment will be discussed here, and the reader is referred to Ref. 2 for further details.

Two pairs of matched 1-in.-diameter quartz transducers, having fundamental frequencies of 0.5 and 1.0 MHz, were used in the acoustic cell shown in Fig. 1 of Ref. 2. In the first set of experiments, the 0.5-MHz crystals were excited at 0.5, 1.0, and 1.5 MHz, and the velocity and attenuation were measured at each frequency along six isochores, including reduced densities ρ/ρ_c of 0.89, 0.96, 1.00, 1.01_5, 1.06, and 1.14. The transducers were held 2.37 mm apart by a rather convoluted spacer, as shown in Fig. 1 of Ref. 2. The idea was to reduce the amount of sound passing through the spacer relative to that through the fluid. In fact, the attenuation became so large close to the critical point that the received pulse through the sample at 1.0 and 1.5 MHz became undetectably small. To correct this problem, the fluid thickness was reduced to 1.33 mm in the 1.0-MHz crystal cell. With this smaller spacing, velocity and attenuation could be measured right up to the critical point at 1.0 MHz, but not at 3.0 or 5.0 MHz.

The capillary through which the ^{3}He sample was inserted into the sample chamber was heated to reduce the amount of residual ^{3}He in the capillary. Although the temperature profile is uncertain, we estimate that less than 0.3% of the sample was in the capillary. Thus, a nearly constant density was achieved by closing a valve to the fill line immediately on top of the cryostat.

The velocity was measured by determining the time of flight of a pulse by a phase comparison technique.[22] The velocity resolution was 10^{-3} m/sec out of 80 m/sec, but the long-term reproducibility was about 10^{-2} m/sec. However, very close to the critical point or where the received amplitude was very small, the reproducibility was only 3×10^{-2} m/sec. The effective acoustic spacing between the transducers and the electronic delay in the time of flight were determined by comparing the measured times of flight in ^{3}He gas at very low pressures with the sound velocity data of Grimsrud and Werntz.[23] We estimate that the *absolute* velocity derived from the effective spacing and time delay correction is accurate to within 0.3 m/sec. However, the dispersion measurements, which rely on *changes* in velocity, are much more accurate, as discussed below. Note that since the time-of-flight method is sensitive to changes in the phase of the received pulse rather than the change in delay of the pulse envelope, the velocity measured is the phase velocity, not the group velocity. These differ by as much as 3% near the critical point because of the large dispersion. The phase velocity will be used throughout this paper.

The attenuation measurements were done with a different technique from that of Garland *et al.*,[7–10] who used a variable-path-length interferometer. Essentially, we measured the amplitude of the received pulse as a function of temperature. The effects of any departure in linearity in the gain of the amplifiers used was eliminated by changing a calibrated step attenuator to keep the received signal amplitude constant, as measured by a boxcar integrator. When the signal became very small at high frequencies near the critical point, the attenuator could not be used, and the attenuation was determined from the calibrated gain curve of the video amplifier. Because the sound velocity of the ^{3}He changes considerably over the experimental temperature range, the acoustic impedance of the fluid changes enough to cause the apparent attenuation to change by several decibels. We have calculated the correction due to this effect (see Appendix A of Ref. 2), and it has been included in all data presented here.

3. RESULTS

Since the method of measuring the received signal amplitude to determine the sound attenuation does not give the absolute acoustic attenuation,

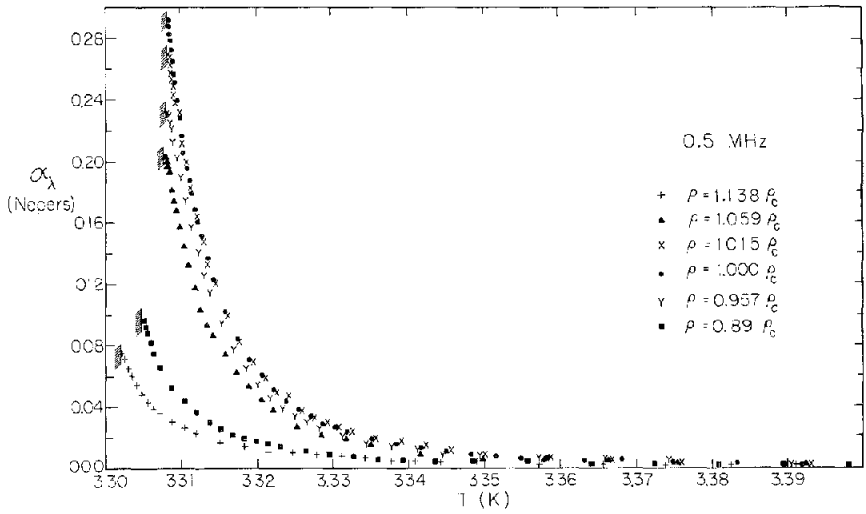

Fig. 1. The singular attenuation $\alpha_{sing}(T)$ along several isochores at the frequency of 0.5 MHz. The vertical line with the hatches indicates the coexistence curve boundary. Data taken beyond $T = 3.40$ K, where $\alpha_{sing}(T)$ is small, are not shown.

we concentrate on the singular attenuation near the critical point and subtract off the small, slowly varying background attenuation due to shear viscosity and thermal conductivity. We write the observed attenuation as

$$\alpha_{obs}(T) = \alpha_{back} + \alpha_{sing}(T) \tag{1}$$

The critical attenuation α_{sing} decreases rapidly as the temperature is raised far above T_c, and for all practical purposes, $\alpha_{obs}(T) = \alpha_{back}$ when T is greater than 3.6 K. After the value of α_{back} to be subtracted from the data has been determined in this way, small self-consistency corrections were made to ensure that α_{sing} is proportional to ω^2 in the hydrodynamic region far from T_c. The critical attenuation calculated in this way is shown along several isochores in Fig. 1. Smoothed data for the attenuation per wavelength $\alpha_\lambda = \alpha\lambda$ along the critical isochore are presented for all our experimental frequencies in Table I. We note that close to T_c, α_λ for 1 MHz becomes systematically smaller than for 0.5 MHz by about 7%. This is slightly different from the experiments for Xe,[11] and also from theoretical expectations.[17] We do not understand what instrumental effects could have caused this small discrepancy at these very high attenuations.

The velocity measurements at 0.5 MHz are presented along several isochores in Fig. 2. Because the electronic time delay depended slightly on the frequency, the time of flight was adjusted so that the velocity was independent of frequency far from T_c ($T > 3.5$ K), where the dispersion is negligible.

TABLE I

Smoothed Ultrasonic Attenuation at Various Frequencies

		Sound attenuation per wavelength α_λ, Np				
T, deg	ε	0.5 MHz	1.0 MHz	1.5 MHz	3.0 MHz	5.0 MHz
3.4737	5.0×10^{-2}	—	—	—	—	0.004
3.4406	4.0×10^{-2}	—	0.002	—	—	0.006
3.4076	3.0×10^{-2}	—	0.003	—	—	0.012
3.3910	2.5×10^{-2}	0.002	0.004	—	—	0.017
3.3745	2.0×10^{-2}	0.003	0.006	—	—	0.026
3.3579	1.5×10^{-2}	0.006	0.011	0.016	0.028	0.043
3.3480	1.2×10^{-2}	0.009	0.016	0.022	0.037	0.057
3.3414	1.0×10^{-2}	0.013	0.022	0.030	0.047	—
3.3348	8.0×10^{-3}	0.020	0.031	0.042	0.063	—
3.3282	6.0×10^{-3}	0.031	0.047	0.061	0.089	—
3.3249	5.0×10^{-3}	0.040	0.060	0.077	0.106	—
3.3216	4.0×10^{-3}	0.054	0.077	0.096	—	—
3.3182	3.0×10^{-3}	0.078	0.101	—	—	—
3.3149	2.0×10^{-3}	0.114	0.135	—	—	—
3.3133	1.5×10^{-3}	0.140	0.159	—	—	—
3.3116	1.0×10^{-3}	0.174	0.186	—	—	—
3.3106	7.0×10^{-4}	0.20	0.21	—	—	—
3.3100	5.0×10^{-4}	0.22	0.22	—	—	—
3.3096	4.0×10^{-4}	0.23	0.23	—	—	—
3.3093	3.0×10^{-4}	0.25	0.24	—	—	—
3.3090	2.0×10^{-4}	0.26	0.25	—	—	—
3.3088	1.5×10^{-4}	0.27	0.26	—	—	—
3.3087	1.0×10^{-4}	0.28	0.26	—	—	—
3.3085	5.0×10^{-5}	0.28	0.27	—	—	—
3.3084	2.0×10^{-5}	0.29	0.27	—	—	—
3.3084	1.0×10^{-5}	0.29	0.27	—	—	—

Unlike ^{4}He (Ref. 3) and Xe (Ref. 7), no low-frequency sound velocity measurements have been reported in ^{3}He. These would have been most useful in determining the dispersion $\Delta U(\omega) = U(\omega) - U(0)$. Instead, we must calculate the limiting zero-frequency (or thermodynamic) velocity from the relation

$$U^2_{\text{therm}}(0) = \frac{1}{\rho K_S} = \frac{1}{\rho K_T} + \frac{T}{\rho^2 C_V}\left(\frac{\partial P}{\partial T}\right)^2_V \tag{2}$$

where K_S and K_T are the adiabatic and isothermal compressibilities, ρ is the mass density, and C_V is the specific heat at constant volume per unit mass. On the critical isochore, we use the available data for K_T,[24] C_V,[20] and $(\partial P/\partial T)_V$[25] to calculate $U_{\text{therm}}(0)$. Unfortunately, however, the combined *systematic* errors in these quantities amount to several percent, which is completely unacceptable for calculating the dispersion to the accuracy of

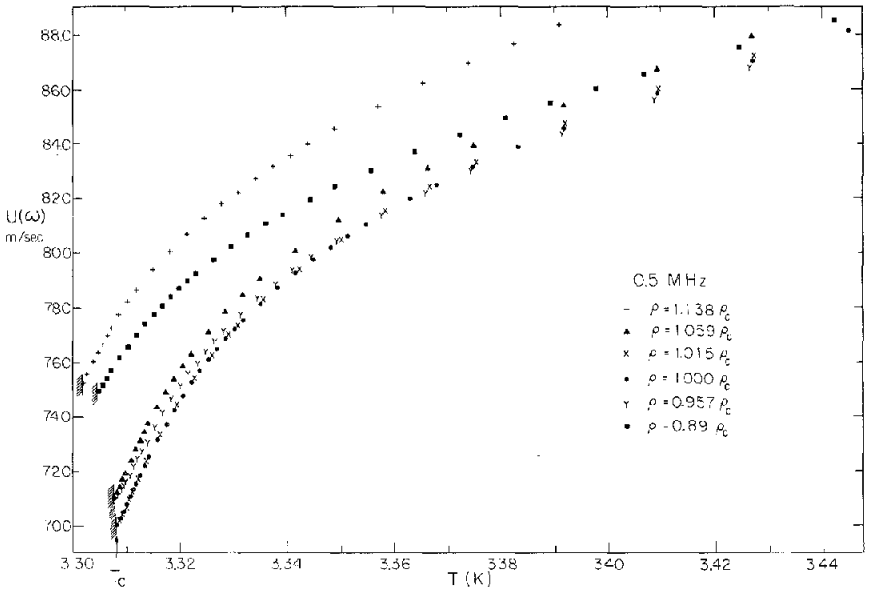

Fig. 2. The sound velocity U along several densities at the frequency of 0.5 MHz. The symbols correspond to the same densities as in Fig. 1 and the coexistence curve boundary is again indicated by the line with the hatches. It is expected that far above the critical region, say at $T > 5$ K, the velocity would increase monotonically as a function of density. This fact explains why the low-density velocity rises less steeply as a function of temperature.

$10^{-3}\,U(0)$. The next step, then, was to adjust the calculated thermodynamic velocity $U_{\text{therm}}(0)$ to fit the measured 0.5-MHz data in the temperature range where the dispersion is small, namely $3.37 < T < 3.53$ K. To preserve the expected weak singularity in $U(0)$, we used the form

$$U(0) = (1-\delta_0)U_{\text{therm}}(0) + \delta_1\varepsilon + \delta_2\varepsilon^2 + \delta_3\varepsilon^3 \tag{3}$$

where $\varepsilon \equiv (T - T_c)/T_c$. The implicit temperature dependence of $U(0)$ and $U_{\text{therm}}(0)$ is understood and the δ_i are free parameters with $|\delta_0| \ll 1$. The difference between $U(0)$ and $U(0.5\text{ MHz})$ is less than 0.01 m/sec throughout the range of the fit. Table II gives $U(0)$ as a function of temperature. It is subtracted from the acoustic velocity to determine the dispersion as a function of temperature and frequency along the critical isochore. Smoothed velocity data at several frequencies are also given in Table II. A technical report tabulating all the velocity and attenuation data is in preparation.

Despite very small transducer separations, gravity-induced density gradients remain a nontrivial problem in our cell very close to the critical point. We can only *estimate* the corrections close to T_c, because the precise

TABLE II

Smoothed Ultrasonic Velocity at Various Frequencies and the Limiting Velocity at Zero Frequency $U(0)$

T, deg	ε	$U(0)$, m/sec	$U(\omega/2\pi)$, m/sec				
			0.5 MHz	1.0 MHz	1.5 MHz	3 MHz	5 MHz
3.5068	6.0×10^{-2}	91.47	91.47	91.47	91.47	91.47	91.48
3.4737	5.0×10^{-2}	89.77	89.77	89.77	89.77	89.78	89.78
3.4406	4.0×10^{-2}	87.89	87.89	87.89	87.89	87.90	89.91
3.4076	3.0×10^{-2}	85.73	85.73	85.74	85.74	85.75	85.76
3.3910	2.5×10^{-2}	84.49	84.49	84.50	84.52	84.53	84.55
3.3745	2.0×10^{-2}	83.08	83.08	83.09	83.11	83.14	83.18
3.3579	1.5×10^{-2}	81.38	81.39	81.41	81.43	81.50	81.58
3.3480	1.2×10^{-2}	80.14	80.16	80.20	80.23	80.34	80.47
3.3414	1.0×10^{-2}	79.17	79.20	79.26	79.31	79.47	—
3.3348	8.0×10^{-3}	78.03	78.09	78.21	78.27	78.53	—
3.3282	6.0×10^{-3}	76.61	76.74	77.00	77.06	77.44	—
3.3249	5.0×10^{-3}	75.74	75.95	76.29	76.39	76.86	—
3.3216	4.0×10^{-3}	74.71	75.03	75.48	75.66	—	—
3.3182	3.0×10^{-3}	73.42	74.00	74.55	—	—	—
3.3149	2.0×10^{-3}	71.68	72.80	73.60	—	—	—
3.3133	1.5×10^{-3}	70.48	72.12	73.09	—	—	—
3.3116	1.0×10^{-3}	68.86	71.40	72.56	—	—	—
3.3106	7.0×10^{-4}	67.47	70.97	72.21	—	—	—
3.3100	5.0×10^{-4}	66.20	70.68	72.00	—	—	—
3.3096	4.0×10^{-4}	65.38	70.54	71.90	—	—	—
3.3093	3.0×10^{-4}	64.34	70.41	71.81	—	—	—
3.3090	2.0×10^{-4}	62.90	70.28	71.71	—	—	—
3.3088	1.5×10^{-4}	61.90	70.22	71.66	—	—	—
3.3087	1.0×10^{-4}	60.53	70.16	71.60	—	—	—
3.3085	5.0×10^{-5}	58.26	70.09	71.55	—	—	—
3.3084	2.0×10^{-5}	55.39	70.05	71.52	—	—	—
3.3084	1.0×10^{-5}	53.32	70.03	71.51	—	—	—

behavior of the velocity and attenuation as a function of density is not known. Nevertheless, as in Appendix B of Ref. 2, we assume that the quadratic density dependence of the velocity and attenuation (see Fig. 3) a few millidegrees above T_c persists even very close to the critical temperature. Then the shift due to gravity is a weighted average of the velocity (or attenuation) over the density profile of the cell. This density profile is calculated[26] as a function of temperature assuming the linear model equation of state.[27] In the cell with 2.37 mm vertical spacing between the quartz transducers, the calculated gravity correction to the velocity increases from 0.035 m/sec at $T-T_c = 1.0$ mK to 0.50 m/sec at the critical temperature, as shown in Fig. 3. The corrections for the cell with 1.33 mm spacing are slightly smaller. The attenuation per wavelength is calculated to be too small by 0.024 Np at T_c in the larger cell.

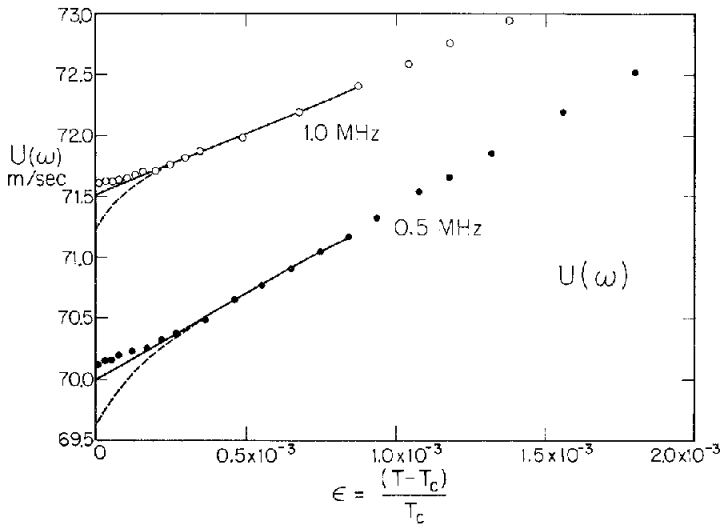

Fig. 3. The velocity at 0.5 and 1.0 MHz along the critical isochore close to T_c. The respective symbols represent the actual data. The dashed curves are the calculated velocity profiles corrected for gravity effects. The solid curves represent the extrapolated velocity data to T_c, which were actually used in the analysis. For explanation of the curves, see text.

Since these calculations of the gravity effect overcorrect for the rounding of the data near T_c, we feel it is possible that the gravity-induced density gradient may not become fully established in the cell. Perhaps the mechanical agitations of the transducers or a slight temperature gradient might produce enough convection in the cell to disturb the formation of the density gradient, thus reducing the correction to the velocity and attenuation. There is some uncertainty in the exact behavior of the velocity and attenuation within 0.5 mK of the critical temperature, but, as a guess, we suppose that they should continue the linear temperature dependence, as in Fig. 3, rather than being cusped, like the calculated corrections, or flattened, like the observed data points. We have therefore used the solid lines in Fig. 3 as the true velocity, and have treated the attenuation in a similar manner. Fortunately, these corrections to the velocity have almost no effect on the dispersion, because the dispersion itself is so much larger than the correction due to gravity. At 0.5 MHz and $\varepsilon = 10^{-5}$, for instance, the dispersion is almost 17 m/sec, but the maximum correction due to gravity is only 0.5 m/sec. In a similar spirit, we have corrected the 0.5-MHz data of the attenuation per wavelength from 0.285 to 0.294 Np at T_c, rather than the calculated correction of 0.310 Np.

4. THEORY, ANALYSIS, AND DISCUSSION

Kawasaki[1] has used the mode coupling formalism to calculate the sound dispersion and attenuation near the liquid–gas critical point, assuming the OZ correlation function. Mistura[15] has derived essentially the same result in terms of a frequency-dependent specific heat, although he has taken into account the Fisher[28] modification of the OZ behavior. The physical idea is that the sound wave requires rapid response from the order-parameter fluctuations in the fluid. If these do not respond as fast as the frequency ω of the sound wave, energy is dissipated, leading to absorption and dispersion. Thus the crucial factor is the ratio $\omega^* = \omega/\omega_D$, where ω_D is the rate of decay by heat diffusion of the characteristic density and entropy fluctuations and

$$\omega_D = 2\Lambda\kappa^2/\rho C_P \tag{4}$$

Here Λ is the thermal conductivity, C_P is the specific heat per unit mass at constant pressure, and κ is the inverse correlation length. Eden *et al.*[9] improved the theory by compensating for the assumption that the dispersion was small compared to the low-frequency velocity. We now review their expressions for sound velocity dispersion and attenuation for a general Fourier-transformed correlation function

$$G(k, \kappa) = \kappa^{\eta-2} f(k/\kappa) \tag{5}$$

where k is the wave number and η is the critical exponent introduced by Fisher.[28] The attenuation per wavelength α_λ and dispersion are given by[11]

$$\alpha_\lambda = \alpha U(\omega)/2\pi\omega = 2\pi A(T) U^2(\omega)\kappa(\partial\kappa/\partial T)_S^2 I(\omega^*) \tag{6}$$

$$U^{-2}(0) - U^{-2}(\omega) = 2A(T)\kappa(\partial\kappa/\partial T)_S^2 J(\omega^*) \tag{7}$$

$$A(T) = (k_B T^3/2\pi^2\rho^3) U^{-4}(0) C_V^{-2} (\partial P/\partial T)_V^2 \tag{8}$$

Since ω^* is very roughly proportional to $\omega^1 \varepsilon^{-2}$, small values of ω^* correspond to the low-frequency hydrodynamic region, while large values correspond to the high-frequency, nonhydrodynamic region close to T_c. Almost all the frequency and temperature dependence of the velocity and attenuation is expressed in terms of functions of the single variable ω^*. These functions, $I(\omega^*)$ and $J(\omega^*)$, are given by definite integrals over the scaled wave number $x = k/\kappa$:

$$I(\omega^*) = \int_0^\infty dx\, [xg(x)]^2 \frac{\omega^* K(x)}{\omega^{*2} + K^2(x)} \tag{9}$$

$$J(\omega^*) = \int_0^\infty dx\, [xg(x)]^2 \frac{\omega^{*2}}{\omega^{*2} + K^2(x)} \tag{10}$$

The function $g(x)$ is related to the logarithmic derivative of the correlation

function $G(k, \kappa)$ by

$$g(x) = 1 - \frac{\eta}{2} + \frac{x}{2f(x)} \frac{df(x)}{dx} \tag{11}$$

and $K(x)$ is the Kawasaki function[31] defined in terms of the decay rate of fluctuations of wave number k,

$$\Gamma(k, \kappa) = (\Lambda \kappa^2 / \rho C_P) K(k/\kappa) = \tfrac{1}{2} \omega_D K(k/\kappa) \tag{12}$$

Kawasaki has calculated an explicit form for $K(x)$ in the OZ approximation:

$$K_0(x) = \tfrac{3}{4}[1 + x^2 + (x^3 - 1/x) \arctan(x)] \tag{13}$$

However, when the effect of the nonlocal high-frequency shear viscosity is taken into account,[30] the behavior of $K(x)$ at large x is considerably modified. From Fig. 3 of Ref. 30, we have inferred the following functional form for $K(x)$, which reproduces the calculated values to within 1% for $x < 30$:

$$K(x) = K_0(x)[1.055^a + (0.93 + 0.29 \log_{10} x)^a]^{1/a} \tag{14}$$

with the fitting exponent $a = 13$. The effect of other corrections to $K(x)$, such as vertex corrections[31] and the departures from the OZ correlation function,[32] are much smaller, and do not have a significant influence on the integrals $I(\omega^*)$ and $J(\omega^*)$. Even the shear viscosity correction[30] changes these integrals by less than 10% for any value of ω^*.

Once the form of the correlation function $f(k/\kappa)$ is specified, the functions $I(\omega^*)$ and $J(\omega^*)$ may be computed via Eqs. (9)–(14). These can then be compared with the *reduced* attenuation and dispersion:

$$\alpha_\lambda [2\pi A(T) U^2(\omega) \kappa (\partial \kappa / \partial T)_S^2]^{-1} = I(\omega^*) \tag{15}$$

$$[U^{-2}(0) - U^{-2}(\omega)][2A(T) \kappa (\partial \kappa / \partial T)_S^2]^{-1} = J(\omega^*) \tag{16}$$

Evaluation of $\kappa(\partial k/\partial T)_S^2$ and the thermodynamic quantities in $A(T)$ is quite tedious in general.[11] On the critical isochore, however, several simplifications occur. First, $(\partial \kappa / \partial T)_S = (\partial \kappa / \partial T)_V$ and $\kappa = \kappa_0 \varepsilon^{\nu}$, so that

$$\kappa \left(\frac{\partial \kappa}{\partial T} \right)_S^2 = \kappa_0^3 \nu^2 \frac{1}{T_c^2} \varepsilon^{3\nu - 2} \tag{17}$$

κ_0 will be treated as an adjustable fitting parameter. Furthermore, the expected divergences of C_V and $U(0)^{-2}$ cancel, so that $A(T)$ is finite and at most cusped at T_c. We have used the data of Refs. 25, 19, and 24 to compute $A(T)$, and find that it decreases by about 15% from T_c to $\varepsilon = 10^{-1}$, mainly because of the increase of $(\partial P/\partial T)_V$ in Eq. (2) as ε increases.

The computation of ω^* via Eq. (4) requires knowledge of ρC_P and Λ. The fact that the second term of the expression

$$\rho C_P = \rho C_V + T(\partial P/\partial T)_V^2 K_T \tag{18}$$

dominates close to T_c due to the strong divergence of K_T allows us to estimate

$$\rho C_P = 9.5 \times 10^4 \varepsilon^{-\gamma} \text{ (J/m}^3\text{-deg)} \tag{19}$$

with the exponent $\gamma = 1.18$, using the data of Refs. 24 and 25.

The thermal conductivity Λ presents more of a problem since the measurements[33] of this quantity in ^{3}He have not particularly focused on the critical region. If the singular and background terms in the thermal conductivity are separated in the form

$$\Lambda = \Lambda_0 \varepsilon^{-\gamma+\nu} + \Lambda_{\text{back}} \tag{20}$$

it is clear from the measurements that the background term is *not* insignificant in our temperature range, and cannot be neglected. The background term Λ_{back} can be estimated to be $(1.55 \pm 0.1) \times 10^{-2}$ W/m-deg. With $\gamma - \nu = 0.55$, we estimate $\Lambda_0 = (8 \pm 4) \times 10^{-4}$ W/m-deg. Considering this uncertainty, it seemed better to use Λ_0 as a second adjustable parameter in the analysis of the acoustic data. Finally, we use this expression to compute ω^*:

$$\omega^* = \omega \rho C_P / [2\kappa_0^2 \varepsilon^{2\nu} (\Lambda_{\text{back}} + \Lambda_0 \varepsilon^{-\gamma+\nu})] \tag{21}$$

where we use Eq. (19) with $\gamma = 1.18$, $\Lambda_{\text{back}} = 1.55 \times 10^{-2}$ W/m-deg, and Λ_0 and κ_0 as adjustable parameters.

We now proceed to the comparison of the reduced attenuation and dispersion [Eqs. (15) and (16)] with the definite integrals $I(\omega^*)$ and $J(\omega^*)$ calculated using different forms of the correlation function. The simplest choice is the OZ form

$$f_{\text{OZ}} = 1/(1+x^2) \tag{22}$$

$$g_{\text{OZ}} = 1/(1+x^2) \tag{23}$$

with $\eta = 0$ in Eq. (11). Since the OZ form is expected to break down for large x, the integrals $I(\omega^*)$ and $J(\omega^*)$ will not represent the data well for large values of ω^*. Accordingly, we have fitted the data only for values of ω^* less than a maximum value ω^*_{max}.

A nonlinear weighted least squares program was used to determine the best values of the two parameters κ_0 and Λ_0 [see Eqs. (17) and (20)]. All other parameters were held constant; in particular, the exponent ν was set equal to the hyperscaling value $(2-\alpha)/3 = 0.63$. The attenuation and dispersion data were always fitted simultaneously to ensure the self-consis-

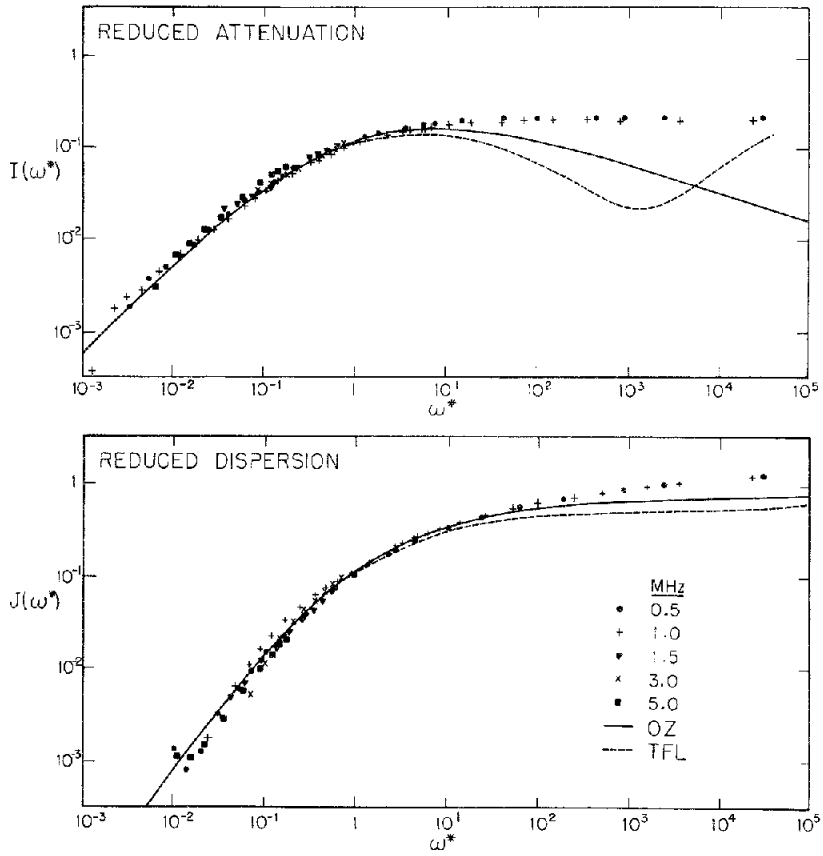

Fig. 4. Fit of the reduced attenuation and dispersion data to the integrals $J(\omega^*)$ and $I(\omega^*)$ of Eqs. (9) and (10). The solid lines represent the integrals using the classical Ornstein–Zernike correlation function, and the dashed lines use the truncated Fisher–Langer correlation function as adapted from the paper by Bray.[20]

tency of the fits to the data. A typical fit to the OZ correlation function, with $\omega^*_{max} = 6.5$, is shown in Fig. 4. The consistency between the attenuation and dispersion data is excellent for $\omega^* < \omega^*_{max}$, and the fit to the calculated integrals is also good in this region. The agreement of the dispersion and attenuation is to some extent a justification of the extrapolated calculation of $U(0)$ used to calculate the dispersion close to T_c. The fit values of the parameters $\kappa_0 = 3.89 \times 10^9$ m^{-1} and $\Lambda_0 = 1.11 \times 10^{-3}$ W/m-deg are consistent with expectations: first, κ_0 should be nearly the same for all fluids,[34] about 5×10^9 m^{-1}, and second, Λ_0 is consistent with our earlier estimation from heat conductivity data, $\Lambda = (8 \pm 4) \times 10^{-4}$ W/m-deg. From the change in the quality of the fit with different values of the parameters κ_0 and Λ_0 and

taking into account the correlation of these variables, we estimate that the possible error in κ_0 is 10% and Λ_0, is 30%.

Ohbayashi and Ikushima[35] have measured both the intensity and linewidth of the Rayleigh-scattered light near the critical point of ^{3}He. From the intensity experiments they find ν and κ_0 as presented in Table IIIB. From their reported value of the high-frequency shear viscosity, one can compute $\Lambda_0 = (5 \pm 2) \times 10^{-4}$ W/m-deg. A direct comparison of these results with ours is difficult because of the different values of ν, but the agreement is not very good.

For different values of the upper limit $\omega^*_{\max}$ of the least squares fit, the values of Λ_0 and κ_0 change slightly, as summarized in Table IIIA. Attempts to fit the data with a still higher cutoff lead to a progressive deterioration of the fit for $\omega^* < 1$, reinforcing the belief that the OZ form does not describe the data in the nonhydrodynamic region $\omega^* \gg 1$. It might be argued that the decrease in reduced absorption very close to T_c and predicted by the OZ correlation function is obscured in this experiment by gravity effects. However, we feel that this predicted decrease should be large enough sufficiently far from T_c that it could not possibly be masked by density inhomogeneity. A similar argument holds for the velocity. For instance, at

TABLE IIIA

Parameters Found in Various Acoustic Experiments in ^{3}He

ν	$\kappa_0 \times 10^9$, m^{-1}	$\Lambda_0 \times 10^{-3}$, W/m-deg	$\omega^*_{\max}$	Correlation function used	Quality of fit for $\omega^* > 10$
0.595	3.31	0.95	∞	OZ	Fair
0.63[a]	3.86	1.08	1.5	OZ	Poor
0.63[a]	3.89	1.11	6.5	OZ	Poor
0.63[a]	3.99	1.26	30.	OZ	Poor
0.63[a]	3.9	1.1	∞	TFL[20]	Very poor
0.63[a]	3.89	1.00	∞	Shown in Fig. 5	Very good

[a]The hyperscaling value $\nu = 2 - \alpha$ is *assumed.*

TABLE IIIB

Parameters Found in Light Scattering and Thermal Conductivity Experiments in ^{3}He

ν	$\kappa_0 \times 10^9$, m^{-1}	$\Lambda_0 \times 10^{-3}$, W/m-deg	Experimental technique	Ref.
0.59 ± 0.04	2.1 ± 0.8	—	Rayleigh scattering intensity	35
0.58 ± 0.05	4.2 ± 1.7	0.5 ± 0.2	Rayleigh linewidth	35
—	—	0.8 ± 0.4	Thermal conductivity	33

$\varepsilon = 2.5 \times 10^{-4}$ the predicted attenuation and velocity at 1.0 MHz are 0.145 Np/wavelength and 70.6 m/sec, respectively, rather than the observed values of 0.247 Np/wavelength and 71.9 m/sec. These differences are well outside the errors ascribable to density inhomogeneities.

As a final attempt to use the OZ form of the correlation function, we allow the exponent ν to be adjustable in the course of the least squares fit, as well as κ_0 and Λ_0. The best values of these parameters fitting *all* the data are $\nu = 0.595$, $\kappa_0 = 3.31 \times 10^9$ m^{-1}, and $\Lambda_0 = 9.51 \times 10^{-4}$ W/m-deg. This fit is, of course, much better in the high-frequency region, but there are still serious discrepancies. Also, the data in the low-frequency region do not fall on a single curve as well as with $\nu = 0.63$. This fit value of $\nu = 0.595$ does *not* reflect a departure from the scaling law $3\nu = 2 - \alpha$, but only the futility of trying to fit the data in the extreme nonhydrodynamic region to the OZ correlation function. This value for ν seems to be quite close to that found by the experimenters in xenon.[8–10]

The task now is to find a functional form for the correlation function $f(x)$ in Eq. (5) that better represents the acoustic data, particularly in the high-frequency region $\omega^* \gg 1$ where the contributions to the definite integrals $I(\omega^*)$ and $J(\omega^*)$ come primarily at large values of $x = k/\kappa$. Hence it is the large-x behavior of $f(x)$ that is of greatest concern. The asymptotically correct form of $f(x)$ for $x \gg 1$ was suggested by Fisher and Langer[18]:

$$f_{\mathrm{FL}}(x) = C_1 x^{-2+\eta}(1 + C_2 x^{-p} + C_3 x^{-1/\nu} + \cdots) \tag{24}$$

where $p \equiv (1-\alpha)/\nu$ and *where C_2 must be greater than zero.* Throughout this paper, we use the notation of Bray.[20] However this form breaks down badly for $x < 1$. Bray has recently computed[20] an approximation to the correlation function for all x, based on a truncation of the Fisher–Langer limiting form (TFL). This calculated correlation function $f_{\mathrm{TFL}}(x)$ as tabulated in Ref. 20 duplicates the OZ correlation function to within 0.1% for $x \ll 1$, and with the exponents $\nu = 0.638$, $\alpha = 0.086$, and $\eta = 0.041$ and parameters $C_1 = 0.909$, $C_2 = 3.593$, and $C_3 = -4.493$ it agrees with the $f_{\mathrm{FL}}(x)$ to within 0.04% for $x > 20$.

To calculate the integrals $I(\omega^*)$ and $J(\omega^*)$ from this correlation function, we have obtained $g_{\mathrm{TFL}}(x)$ by differentiating an analytic approximation to the tabulated $f_{\mathrm{TFL}}(x)$ in the range $0.2 < x < 20$. The definite integrals are evaluated from $g_{\mathrm{TFL}}(x)$ by Gaussian quadrature. Unfortunately, since $g_{\mathrm{TFL}}(x)$ passes through zero and becomes negative at $x = 10.3$, the factor $[x g_{\mathrm{TFL}}(x)]^2$ appearing in the integrals also reaches zero at this point. This results in a minimum in $I(\omega^*)$ and an inflection in $J(\omega^*)$ at $\omega^* \approx 10^3$, as shown in Fig. 4. Thus, these calculated integrals do *not* describe the data better than those using the OZ correlation function. In fact, the fit is worse! In general, *any* correlation function that approaches the Fisher–Langer

form for large x will produce a root in $g_{\mathrm{TFL}}(x)$ for some intermediate value of x, because $g_{\mathrm{TFL}}(x)$ calculated via Eq. (11) from $f_{\mathrm{FL}}(x)$ is negative for large x when $C_2 > 0$. This function is given by

$$g_{\mathrm{FL}}(x) = \frac{-pC_2x^{-p} - (C_3/\nu)x^{-1/\nu}}{2(1 + C_2x^{-p} + C_3x^{-1/\nu})} \tag{25}$$

This root in $g(x)$ is responsible for lower values of $I(\omega^*)$ and $J(\omega^*)$, resulting in a poorer fit than with $g_{\mathrm{OZ}}(x)$ and the agreement with the experimental data is poor in the intermediate region $10 < \omega^* < 10^3$. However, the *asymptotic* behavior of the Kawasaki–Mistura equations using the Fisher–Langer form [Eq. (24)] for $\omega^* \gg 10^3$ is identical to the general prediction of Kawasaki, namely

$$\alpha_\lambda \propto \varepsilon^{-3\alpha/2}\omega^{\alpha/3\nu} \approx \varepsilon^0\omega^0 \quad \text{and} \quad \Delta U \propto \varepsilon^{-\alpha/2}\omega^{\alpha/3\nu} \approx \varepsilon^0\omega^0 \tag{26}$$

The approximate relation is reasonable since α is very small. These predictions are qualitatively consistent with acoustic experiments in Xe,[11] ^{4}He,[2] and ^{3}He as well as Brillouin scattering experiments in Xe.[13] However, the failure of the Fisher–Langer form to give even the same *qualitative* form for the dispersion and attenuation as observed in the intermediate frequency range is not understood. Certainly in the Fisher–Langer asymptotic form [Eq. (24)] C_2 must be positive for thermodynamic reasons.[36] †

We now introduce an *empirical* form for $f(x)$, which we denote by $f_A(x)$, namely

$$f_A(x) = (1 + x^2)^{-1}[1 - C_2'x^{-p} \exp(C_2'/x)]^{-1} \tag{27}$$

This form was taken because it gives a smooth behavior for the derivative $g_A(x)$, from which the integrals $I(\omega^*)$ and $J(\omega^*)$ are computed,

$$g_A(x) = \frac{1}{1+x^2} - \frac{1}{2}C_2'x^{-p}\frac{p + C_2'x^{-1}}{[\exp(-C_2'/x)] - C_2'x^{-p}} \tag{28}$$

This form reduces to the OZ form [Eq. (23) for small x. For large x, the form is similar to the Fisher–Langer form with only the *dominant* term, if we identify C_2 with C_2'. However, our best fit gives $C_2' = -0.46$ and hence our empirical form should *not* be identified with the Fisher–Langer expression.

In Fig. 5, we compare the various forms for $xg(x)$ used to fit experimental results. First, we show the OZ form [Eq. (23)]; second, the truncated Fisher–Langer (TFL) form as derived from Bray's correlation function; third, the form as obtained by Tartaglia and Thoen from their fit to the xenon data (Xe), and finally, that obtained from a fit using Eq. (28) in the present

†The constant C_2 and its sign are found to be closely related to the amplitude of the specific heat singularity, which has to be positive. The signs of the higher order terms C_3, etc., are not as definite, however.

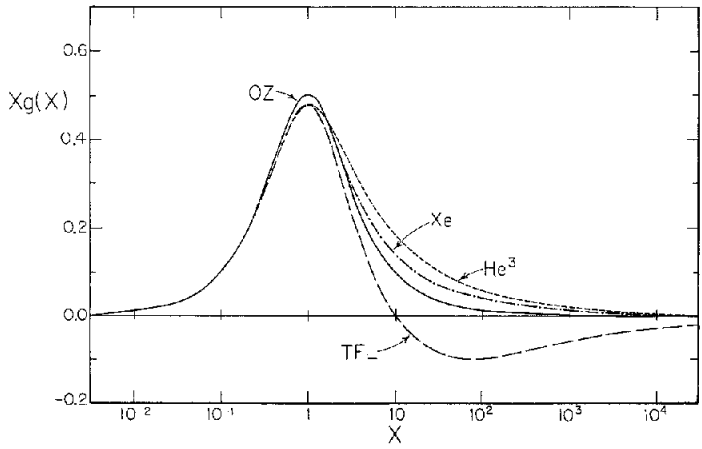

Fig. 5. A comparison of the function $xg(x)$ from Eq. (11) obtained from various models. (——) Ornstein–Zernike [Eq. (23)]. (– – –) Truncated Fisher–Langer (TFL) derived from Table 5 of Ref. 20. (–·–) Fisher–Langer but with $C_2 = -0.63$, as constructed by Tartaglia and Thoen (Xe) in their Fig. 1. (- - -). Function constructed in this paper (^{3}He) with $C_2 < 0$, $\eta = 0.0$ to fit the ^{3}He data.

work (^{3}He). The fit of theory using Eq. (28) is shown in Fig. 6. Perhaps it is not coincidental that the same function $g(x)$ gives excellent agreement for *both* dispersion and attenuation. It is clear that in order to give a good fit, $xg(x)$ has to be larger than the OZ form for intermediate values $5 < x < 100$.

Analysis of the acoustic and optical data in xenon has been carried out[16] in terms of the Fisher–Langer form. In that analysis, a different sign convention than in other work[18,20,21,32] has been chosen for the constants C_2 and C_3 and this has apparently led to confusion, particularly in references to earlier work.† The Fisher–Langer *asymptotic* form, containing only the two correction terms with C_2 and C_3, was smoothly joined to the OZ form. This composite function was used to fit the Xe data over a wide range of x.[16] The coefficients C_2 and C_3 must then be looked upon as *empirical* parameters and cannot be given theoretical significance. Hence, the form taken by Tartaglia and Thoen to fit their data is in reality *empirical* and not related to Fisher–Langer, especially because they found C_2 to be negative.

A value of $\nu = 0.60$ was used in the analysis of the xenon data, which seems to be too low, since the hyperscaling value is $\nu = (2-\alpha)/3 = 0.625 \pm 0.005$, taking $\alpha = 0.125$,[38] and the three-dimensional Ising model series expansions[39] give $\nu = 0.638 \pm 0.002$. This choice of $\nu = 0.60$ accounts to some extent for the drop of the experimental reduced attenuation for

†Ref. 16 quotes Fisher and Aharony[21] as reporting $C_2 \approx -2$ and $C_3 \approx 3$ (in our notation!), which are the incorrect signs.

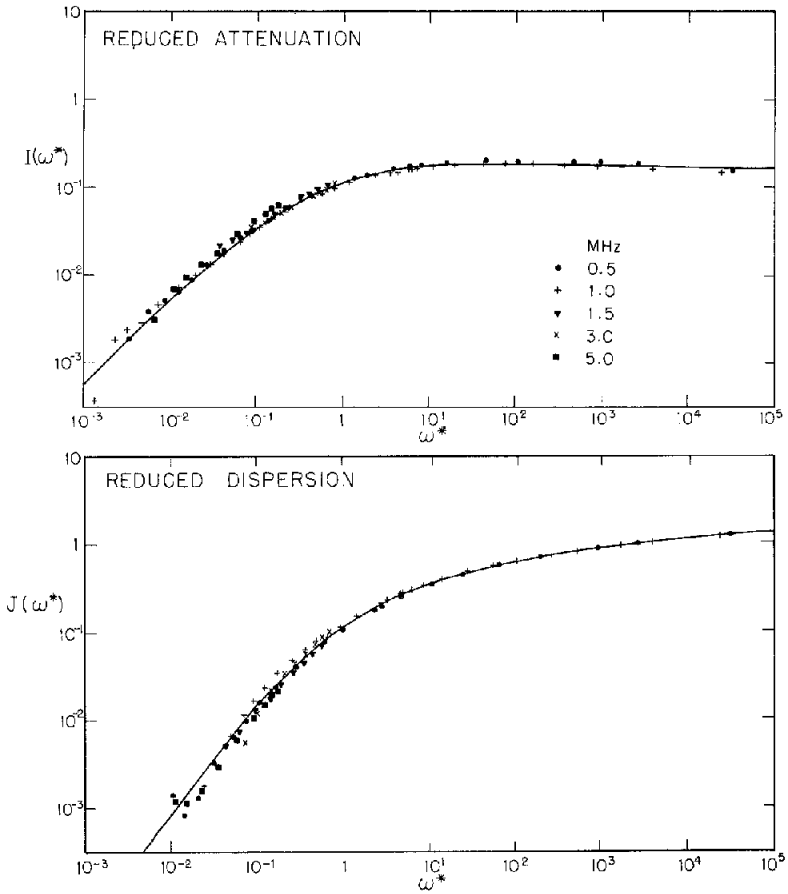

Fig. 6. Fit of the reduced attenuation and dispersion data to the integrals $I(\omega^*)$ and $J(\omega^*)$. The solid lines represent the integrals using the function $xg(x)$, labeled ^{3}He, shown in Fig. 5.

$\omega^* > 10$ in Fig. 8 of Ref. 11. However, the choice of $\nu = 0.63$ subsequently used in analysis by Sarid and Cannell (Fig. 6 of Ref. 37) does not seem to alter drastically the shape of the data profile. In ^{3}He, as well as in ^{4}He, there appears to be no maximum in the reduced attenuation data plot.

Very recently Sarid and Cannell[37] presented a new analysis of acoustic and optical data in terms of the Kawasaki and the Mistura theory. In their comparison, they used the form for $xg(x)$ used by Tartaglia and Thoen under the label "Fisher–Langer," and our remarks made above also apply to their paper. One of the principal results of Ref. 37 is that when taking the best values available from optical and thermodynamic sources—that is, not using adjustable parameters—to calculate the attenuation and dispersion,[8] there

is a disagreement by a factor of about two between experiment and theory. In ^{3}He and ^{4}He the values of κ_0 and Λ obtained elsewhere might not be as reliable as in Xe, yet the κ_0 values obtained from a fit are consistent with those of other fluids. Hence, our experiments at this time cannot prove nor disprove the conclusions in Ref. 37.

5. CONCLUSION

We have presented data of the acoustic attenuation and dispersion in ^{3}He at megahertz frequencies and we have analysed the results along the critical isochore in terms of the Kawasaki theory as extended by Mistura. For this analysis we used the available measurements of thermodynamic quantities but were hampered by lack of accurate information on the singular part $\Lambda_0\varepsilon^{-\gamma+\nu}$ of the thermal conductivity. In fitting the theory to our experiments, the free parameters were taken to be Λ_0 and κ_0, the amplitude of the inverse correlation length. The exponent ν was taken to be 0.63, the hyperscaling value.

We have elaborated considerably on the form of the fluctuation correlation function and its logarithmic derivative $g(k/\kappa)$, the latter entering prominently in the Kawasaki formulation. We discussed the fit of the theory using the classical Ornstein–Zernike (OZ) function, that by Fisher and Langer (FL), and the truncated Fisher–Langer function (TFL) as proposed by Bray. In the last two functions, we were especially concerned with the "universal" constant C_2 (in Bray's notation), which has to be positive for very direct physical reasons.

Our results can be summarized as follows:

1. In the low-frequency regime, characterized by $\omega^* = \omega/\omega_D < 10$, where ω_D is a characteristic thermal diffusion rate, theory for both attenuation and dispersion can be fit very well to the ^{3}He data using the OZ correlation function. The same parameter values for κ_0 and Λ_0 fit both experiments, and these values are consistent with expectations. The same analysis has been carried out for ^{4}He with similar conclusions, as discussed in the appendix. Comparison with light scattering experiments show good consistency in κ_0 with Tominaga's data in ^{4}He, but only fair agreement with those of Ikushima's group for both ^{3}He and ^{4}He.

2. The analysis for ^{3}He has been extended into the intermediate frequency regime $\omega^* < 10^3$ by using the TFL function of Bray. It was discovered, however, that a satisfactory fit with the positive C_2 was not possible.

3. An excellent fit for ^{3}He over the whole frequency range was, however, achieved for both attenuation and dispersion when an empirical form for $xg(x)$ was used, the leading term of which corresponded to C_2

negative—an unphysical assumption. Hence, the Fisher–Langer form with $C_2 > 0$, combined with the Mistura theory, is not in agreement with the data. A similar empirical function $xg(x)$ was obtained for xenon by Tartaglia and Thoen, who, however, had claimed agreement with the Fisher–Langer form. Although no such analysis has been made for ^{4}He, the great similarity of the reduced attenuation and dispersion data to those of ^{3}He strongly indicates that a fit will also be equivalent to having a negative C_2 in the Fisher–Langer form.

Thus the question is brought up as to why the experimental data in fluids give worse agreement with the Kawasaki–Mistura theory using an improved decay correlation function by Fisher–Langer than using the classical Ornstein–Zernike form. The empirical function $xg(x)$ that is required to fit the data in the high-frequency region is substantially different from the presumably correct Fisher–Langer form for values of the variable $k/\kappa > 1$. We conclude that the mode-coupling theory in its present form is unable to account for the acoustic data in the high-frequency region. We hope that the existing experiments in fluids will stimulate research to clarify this problem.

We finally mention that no analysis of the data has been made at densities other than the critical one, because of the uncertainty in the thermal conductivity data. Such measurements are planned in the near future, after which we intend to return to complete the analysis of the acoustic data.

APPENDIX. REANALYSIS OF THE ^{4}He ACOUSTIC DATA NEAR THE LIQUID–GAS CRITICAL POINT

In Ref. 2, the acoustic dispersion and attenuation on the critical isochore near the ^{4}He critical point was analyzed using the modification[9] of the Kawasaki–Mistura[1,15] theory, but without taking into account the nonsingular term Λ_{back} in the thermal conductivity [see Eq. (20)]. The singular part $\Lambda_{\text{sing}} = \Lambda_0 \varepsilon^{-\gamma+\nu}$ was implicitly assumed to be much larger than Λ_{back} for all temperatures, while in fact we estimate that this is true only for $\varepsilon < 5 \times 10^{-3}$. Hence the background term is likely to be important in ^{4}He, especially relatively far from T_c. Here we reanalyze the previously published data. Only the OZ correlation function, Eqs. (22) and (23), will be used, however.

The reduced attenuation and dispersion are calculated as in ^{3}He, using Eqs. (15) and (16). The thermodynamic velocity $U(0)$ is found from Ref. 3, as shown in Eqs. (2a) and (2b) and in Table 1 of Ref. 2. The quantity $A(T)$ is assumed to be constant close to T_c, because

$$U^2(0) C_V = (T_c/\rho_c^2)(\partial P/\partial T)_V^2 \approx \text{const} \tag{A1}$$

This gives

$$A(T) = (k_B T_c \rho_c / 2\pi^2)(\partial P/\partial T)_V^{-2} \tag{A2}$$

Using the thermodynamic parameters[40]

$$T_c = 5.189 \text{ K}, \qquad \rho_c = 0.0696 \text{ g/cm}^3$$
$$(\partial P/\partial T)_{\rho=\rho_c} = 1.727 \times 10^5 \text{ J/m}^3\text{-deg}$$

we find

$$A(T) = 8.5 \times 10^{-33} \text{ m/sec}^2$$

For the reduced frequency ω^*, we use

$$\rho C_P = 1.54 \times 10^{-3} \varepsilon^{-\gamma} \text{ J/m}^3\text{-deg}$$

with $\gamma = 1.18$, derived from a combination of data of C_V, $(\partial P/\partial T)_\rho$, ρ_c, and k_T via Eq. (18). As in the ^{3}He analysis, we set

$$\Lambda = \Lambda_{\text{back}} + \Lambda_0 \varepsilon^{-\gamma+\nu} \tag{A3}$$

However, there are no thermal conductivity data in the critical region of ^{4}He to estimate Λ_{back} from. Hence, in the absence of better information, we estimate Λ_{back} from the relation

$$\Lambda_{\text{back}}(\rho_c, T_c) = \Lambda(\rho = 0, T_c) + \delta\Lambda \tag{A4}$$

where $\Lambda(\rho = 0, T_c)$ is found to be 1.05×10^{-2} W/deg-m from the low-pressure data of Ubbink[41] and Kerrisk and Keller,[33] and $\delta\Lambda$ is estimated to

TABLE IV

The Parameters Obtained from a Least Squares Fit of Acoustic Dispersion and Attenuation in ^{4}He Near the Liquid–Gas Critical Point

$\omega^*_{\max}$ used in fit	Dispersion data			Attenuation data	
	ν	$\kappa_0 \times 10^{-9}$, m^{-1}	$\Lambda_0 \times 10^3$, W/m-deg	$\kappa_0 \times 10^{-9}$, m^{-1}	$\Lambda_0 \times 10^3$, W/m-deg
1.5	0.72	9.7	4.0	9.2	4.4
4	0.66	6.7	2.2	6.4	1.9
10	0.63[a]	5.5	1.65	5.4	1.33
15	0.62	5.2	1.5	5.1	1.2

[a]Here ν was *fixed* at 0.63.

be 2.5×10^{-3} W/deg-m based on the density dependence of the background thermal conductivity of ^{3}He, which increases about 25% from $\rho = 0$ to $\rho = \rho_c$. Thus

$$\Lambda_{\text{back}}(\rho_c, T_c) = 1.3 \times 10^{-2} \text{ W/deg-m} \tag{A5}$$

There is a systematic discrepancy between the OZ model and this experiment for $\omega^* > 5$. This causes, as in ^{3}He, a systematic dependence of the free parameters upon the upper limit $\omega^*_{\max}$ of the data used in the fit. Three free parameters (ν, κ_0, and Λ_0) were used for a fit of the dispersion data for a variety of values $\omega^*_{\max}$ and their values are listed in Table IIIA. The variation of the exponent ν with different values of $\omega^*_{\max}$ indicates that it is not possible to find the "best" value of ν by fitting to the OZ correlation function. However, we do *not* find within the range of acceptable fitting the value of $\nu = 0.54$ reported in Ref. 6. To reduce the number of free parameters, we fix ν at the scaling value of $\nu = 0.63$. Then, with $\omega^*_{\max} = 10$, we obtain

$$\kappa_0 = (5.5 \pm 1.0) \times 10^9 \text{ m}^{-1}$$

$$\Lambda_0 = (1.65 \pm 0.3) \times 10^{-3} \text{ W/deg-m}$$

The estimated errors do not take into account possible uncertainties in ν, Λ_{back}, or in any of the other input numbers.

For the attenuation data, where a smaller range of frequencies was covered, we have assumed the same values of ν found from the dispersion fit for a given $\omega^*_{\max}$. The results for the remaining free parameters κ_0 and Λ_0 are given in Table IV. Generally, they are in close agreement with those from the dispersion fit, which indicates an encouraging consistency between the

TABLE V

Comparison of the Parameters from Acoustic Experiments with Those from Light Scattering Data in ^{4}He

ν	$\kappa_0 \times 10^{-9}$, m^{-1}	$\Lambda_0 \times 10^3$, W/m-deg	Method	Ref.
0.63[a]	5.5	1.65	Acoustic dispersion	This work
0.62 ± 0.1	4.4 ± 1.2	—	Scattering intensity	5
0.59 ± 0.02	1.4 ± 0.4	—	Scattering intensity	4
0.54 ± 0.05	2.8 ± 0.6	—	Scattering linewidth	6
0.67 ± 0.02	2.9 ± 0.2	—	Scattering intensity	42

[a]Used as input; when ν is used as a free parameter, we obtain the values shown in Table IV.

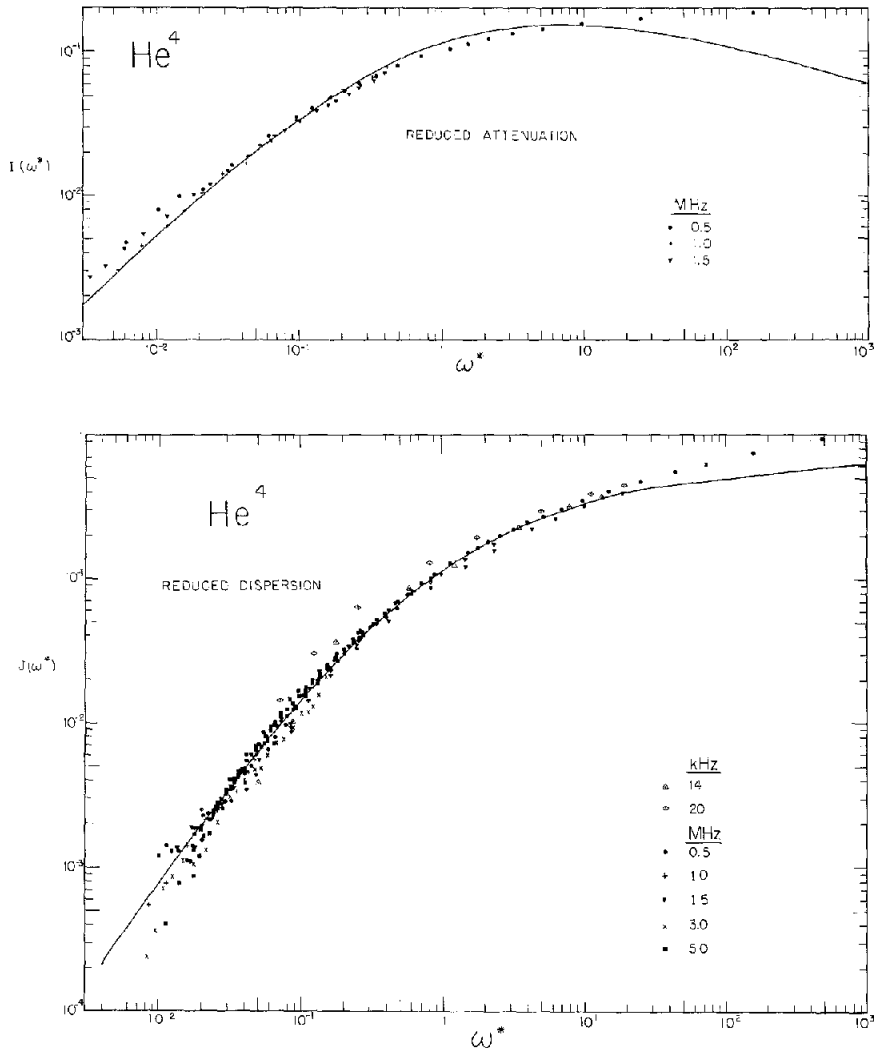

Fig. 7. The reduced dispersion and attenuation, as calculated from Eqs. (15) and (16), in ^{4}He. The solid lines represent the integrals $I(\omega^*)$ and $J(\omega^*)$, found by assuming the OZ correlation function. The parameters used in each graph are $\nu = 0.66$, $\kappa_0 = 6.74 \times 10^9$ m^{-1}, and $\Lambda_0 = 2.23 \times 10^{-3}$ W/m-deg. The low-frequency dispersion data of Barmatz[3] are also shown. These graphs may be compared to Figs. 6 and 7 of Ref. 2; the closer agreement in the present fit is evident far from T_c, where the background term in Λ is significant.

two types of experiments. Figure 6 shows a representative fit with the same parameters, for both dispersion and attenuation. The quality of the fits is not markedly different for the various choices of $\omega^*_{\max}$ in Table IIIA. These fits

should be compared with Figs. 6 and 7 of Ref. 2. See Fig. 7. Note that the low-frequency dispersion data of Barmatz[3] are now in substantially better agreement with ours. Hence the scaling fit covers the impressive range from 14 kHz to 5 MHz!

Our values of the resulting fit parameters are compared in Table V with those from light scattering experiments,[4,5,6,40] and we note the good agreement for κ_0 with the result by Tominaga[5] and the consistency with κ_0 found in other fluids.[34]

ACKNOWLEDGMENTS

The authors are very indebted to Prof. M. E. Fisher for his clarification of the Fisher–Langer correlation function. They are grateful to Prof. C. Garland for his helpful comments on the manuscript and to Drs. Tartaglia and Thoen for correspondence on their analysis.

REFERENCES

1. K. Kawasaki, *Phys. Rev. A* **1**, 1750 (1970).
2. D. Roe, B. Wallace, and H. Meyer, *J. Low Temp. Phys.* **16**, 51 (1974).
3. M. Barmatz, *Phys. Rev. Lett.* **24**, 651 (1970); M. Barmatz, in *Proc. Battelle Colloq. on Crit. Phen.* (Gstaad, 1970) (McGraw-Hill, New York, 1972), p. 541.
4. S. Kagoshima, K. Ohbayashi, and A. Ikushima, *J. Low Temp. Phys.* **11**, 765 (1973).
5. A. Tominaga, A. Nakazawi, and Y. Narahara, *Phys. Lett.* **46A**, 383 (1974); and A. Tominaga, *J. Low Temp. Phys.* **16**, 571 (1974).
6. K. Ohbayashi and A. Ikushima, *J. Low Temp. Phys.* **15**, 33 (1974).
7. C. Garland and R. Williams, *Phys. Rev. A* **10**, 1328 (1974).
8. C. Garland, D. Eden, and L. Mistura, *Phys. Rev. Lett.* **25**, 1161 (1970).
9. D. Eden, C. Garland, and J. Thoen, *Phys. Rev. Lett.* **28**, 726 (1972).
10. P. Mueller, D. Eden, C. Garland, and R. Williamson, *Phys. Rev. A* **6**, 2272 (1972).
11. J. Thoen and C. Garland, *Phys. Rev. A* **10**, 1311 (1974).
12. D. Henry, H. Swinney, and H. Cummins, *Phys. Rev. Lett.* **25**, 1170 (1970).
13. D. Cannell and G. Benedek, *Phys. Rev. Lett.* **25**, 1157 (1970).
14. H. Cummins and H. Swinney, *Phys. Rev. Lett.* **25**, 1165 (1970).
15. L. Mistura, in *International School of Physics 'Enrico Fermi' Course LI*, M. S. Green, ed. (Academic Press, New York, 1971), p. 563.
16. P. Tartaglia and J. Thoen, *Phys. Rev. A* **11**, 2061 (1975).
17. K. Kawasaki, *Phys. Rev. A* **3**, 1097 (1971).
18. M. E. Fisher and J. Langer, *Phys. Rev. Lett.* **20**, 665 (1968).
19. R. Brown and H. Meyer, *Phys. Rev. A* **6**, 364 (1972).
20. A. Bray, *Phys. Lett. A* **55**, 453 (1976); *Phys. Rev. B* **14**, 1248 (1976).
21. M. Fisher and A. Aharony, *Phys. Rev. Lett.* **31**, 1238 (1973).
22. R. Wanner, K. Mueller, and H. Fairbank, *J. Low Temp. Phys.* **11**, 363 (1973).
23. D. Grimsrud and J. Werntz, *Phys. Rev.* **157**, 181 (1967).
24. B. Wallace and H. Meyer, *Phys. Rev. A* **2**, 1563 (1970).
25. R. Behringer, T. Doiron, and H. Meyer, *J. Low Temp. Phys.* **24**, 315 (1976).
26. P. Hohenberg and M. Barmatz, *Phys. Rev. A* **6**, 289 (1972).
27. P. Schofield, J. Litster, and J. Ho, *Phys. Rev. Lett.* **23**, 1098 (1969).
28. M. E. Fisher, *J. Math. Phys.* **5**, 944 (1969).

29. K. Kawasaki, *Ann. Phys. (N.Y.)* **61**, 1 (1970).
30. K. Kawasaki and S. Lo, *Phys. Rev. Lett.* **29**, 48 (1972).
31. H. Swinney and D. Henry, *Phys. Rev. A* **8**, 2586 (1974).
32. C. Tracey, *Phys. Lett.* **48A**, 9 (1974).
33. J. Kerrisk and W. Keller, *Phys. Rev.* **177**, 341 (1969).
34. J. V. Sengers and J. H. M. Levelt Sengers, in *Progress in Liquid Physics*, C. A. Croxton, ed. (Wiley, New York, 1976).
35. K. Ohbayashi and A. Ikushima, *J. Low Temp. Phys.* **19**, 449 (1974).
36. M. E. Fisher, private communication.
37. D. Sarid and D. S. Cannell, *Phys. Rev. A* **15**, 735 (1977).
38. F. van Kann, Ph.D. Thesis, Univ. of Western Australia, unpublished (1975).
39. M. Moore, D. Jasnow, and M. Wortis, *Phys. Rev. Lett.* **22**, 940 (1969).
40. H. Kierstead, *Phys. Rev. A* **3**, 329 (1971).
41. J. Ubbink, *Physica* **13**, 659 (1947).
42. A. Koenig, Ph.D. diss., Duke Univ. unpublished (1974).